Hindawi
Shock and Vibration
Volume 2018, Article ID 5974759, 13 pages
https://doi.org/10.1155/2018/5974759

Research Article

Vibratory Power Flow Analysis of a Gear-Housing-Foundation Coupled System

Yafeng Ren[1], **Shan Chang**[1,2], **Geng Liu**[1], **Liyan Wu**[1] and **Haiwei Wang**[1]

[1] *Shaanxi Engineering Laboratory for Transmissions and Controls, Northwestern Polytechnical University, 710072, China*
[2] *Harbin No. 703 Research Institute of CSIC, 150078, China*

Correspondence should be addressed to Geng Liu; npuliug@nwpu.edu.cn

Received 12 December 2017; Accepted 10 June 2018; Published 28 June 2018

Academic Editor: Nicola Nisticò

The marine gearbox is usually installed on a vibration isolation system in order to reduce oscillation transmitted to the ship foundation. However, researches on vibration transmission in the gear-housing system and isolation system are currently independent. With the increasing requirement of lower vibration, a coupled model needs to be built to control the vibration propagation from a view of the whole system. Considering the mesh transmission error excitation of a gear pair, a flexible gear-housing-foundation coupled impedance model is constructed in this paper, and the vibratory power flow of the whole system is calculated. Power transmissions between three different gearbox installation configurations, that is, rigid installation, single-stage isolation, and double-stage isolation, are compared. Taking the single-stage isolation configuration as an example, parameter influences on the vibration of the foundation are studied. Results show that double-stage isolation can achieve lower vibration than single-stage isolation; decrease in bearing stiffness or Young's modulus of isolator will yield better vibration isolation performance; housing damping and isolator damping are beneficial to vibration reduction.

1. Introduction

Vibration and noise of a ship will not only decrease the comfort of the seaman in the cabin but also throw a terrible threat to the marine creature. In order to reduce the vibration transmitted to the ship foundation, a marine gearbox is often installed on the raft or ship foundation through isolators. Vibration isolation system will influence the dynamic response of gearbox, and the geared transmission system and housing will in turn affect the isolation performance. Many researchers have studied the gear mesh stiffness, many have studied the dynamic response or vibration transmission of a gear-housing system, and many others have studied the vibration transmission in common isolation systems. However, a whole gear-housing-foundation coupled model is seldom reported.

Mesh stiffness is one of the main research aspects of gear dynamics. Kiekbusch [1] simulated the torsional mesh stiffness using two- and three-dimensional finite element (FE) models. Parker [2] proposed a combined FE and contact mechanics model to predict tooth deformation. Chang [3] coupled the gear manufactory error with mesh stiffness during the calculation of static transmission error and mesh stiffness in the loaded tooth contact analysis model. Wang [4] analyzed the mesh stiffness based on the thin slice theory. Song [5] believes that the operating gear centre distance will deviate from its nominal value for a flexible supported gear set. And he used a FE model to evaluate the gear mesh stiffness with varying gear centre distance.

Dynamic response of the gear-housing system has been extensively studied. Ren [6] reviewed gear dynamic analyses considering housing compliance and proposed the impedance synthesis method to study the influence of housing compliance on transmission system. Yang [7] extracted the lumped parameter of the housing from an appropriate set of frequency response functions and simulated the dynamic response of hypoid gearbox. Liu [8] studied the dynamic characteristic of gear-housing system based on the ADAMS software. Xu [9] investigated the influence of housing flexibility on the dynamic response and load sharing among the planetary gears. Some researchers have studied the vibration transmission in a gear-housing system. Guo

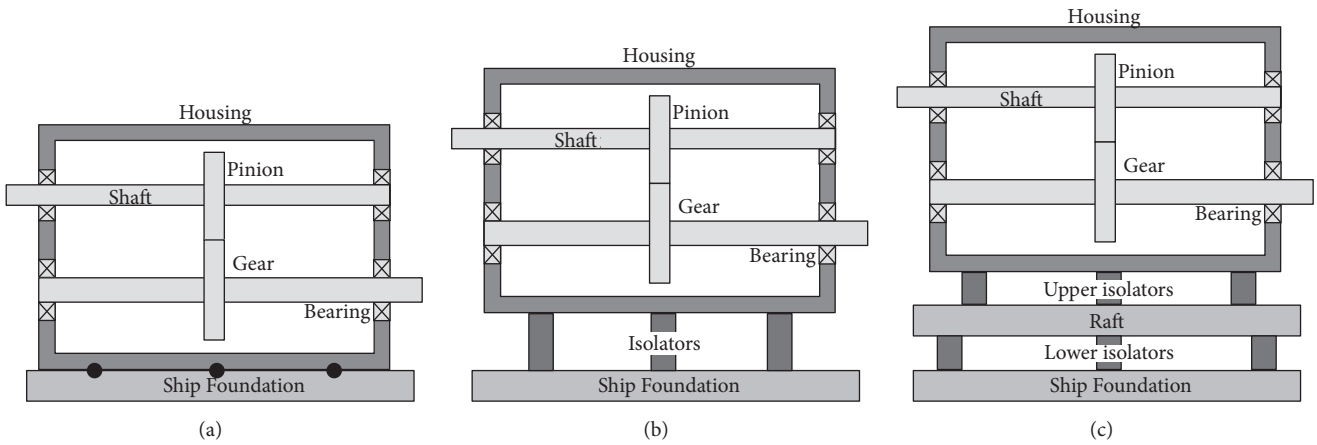

Figure 1: Schematic of typical gearbox isolation configurations: (a) rigid installation; (b) single-stage isolation; (c) double-stage isolation.

[10] measured the frequency response function of the system. Lim [11] analyzed the bearing transmissibility in a shaft-bearing-casing-mount system. Xiao [12] studied the vertical vibration transmission and energy dissipation of the gear-housing system under the impulse force excitation due to gear fault. Rook [13] calculated the vibratory power flow through bearings in a gear-shaft-bearing-rigid casing-mount system and identified some concepts to reduce noise and vibration. Leung [14] claimed that gear tangential forces transmit most of the vibratory power to the housing.

Vibration transmission in general isolation systems is also extensively studied. Research objects have been developed from rigid models [15, 16] to flexible ones [17–19], and the performance index has been developed from force or velocity indices [20–22] to power flow indices [17, 18, 23]. Du [24] found that the force transmissibility increased 20~30 dB, and the noise radiated by the foundation increased about 22 dB when wave effects of isolators are considered. Sanderson [25] emphasized the effects of rotational degree of freedom (DOF) on the total power transmission. Petersson [26] addressed the need to consider both the multimount and the multidirectional vibration transmission in the analysis. Li [27] compared the transmitted reaction force and power flow in an isolator system and pointed out that power flow is more reasonable as a performance index especially at high frequencies. Weng [28] and Sun [29] studied the relationship between power flow transmissibility and vibration acceleration level difference. Singh [30] examined some common vibration isolation measures and showed the close relationship between structural noise emission and the transmitted power. Many authors have adopted power minimization as the control strategy for active isolation system and semiactive isolation system [31–33].

Even though many papers have studied the vibration transmission in a gear-housing system or in a general isolation system, they seldom report about vibration propagation in a gear-housing-foundation coupled system. Some of them treated the housing as a pure spring, and some treated the gearbox as a rigid mass and applied an assumed unit excitation force on it. These models cannot predict the vibration transmission in a gear-housing-foundation system exactly. Though a continuum FE model can be used in a gear-housing system, this method can hardly be adopted in a gear-housing-foundation system because of the large mode truncation error and the great amount of calculation. Lim [11] built a 12-DOF lumped parameters model to study the vibration transmission of a rigid shaft–bearing-rigid plate–mount system. He analyzed the system modes and frequency responses and compared his model with a 2-DOF one. Rook [13] built a mobility model for a rigid gear-shaft-bearing-rigid casing-mount system. However, his model is still very simple, and the dimension of the mobility matrix is only 8. In this paper, a multimount, multidirectional, and flexible gear-housing-foundation coupled impedance model is constructed, the transmission error excitation simulated from a loaded tooth contact analysis model is applied on the gear pair, and then the vibratory power flow is studied.

2. System Modeling

A marine gearbox was often rigidly mounted on the ship foundation in the past, as shown in Figure 1(a). With the vibration isolation applied to the engines, the structure-borne noise of gearboxes is gradually outstanding. In order to reduce vibration and noise of the ship, gearboxes are installed on the ship foundation through single-stage isolation system or double-stage isolation system, as shown in Figures 1(b) and 1(c), respectively.

The double-stage isolation case is used here to describe the modeling process due to its generality. The whole system contains a gear pair, two shafts, four bearings, a housing, twelve isolators, a raft, and a foundation. Since multidirectional flexible model can better characterize the vibration transmission than others, subsystems are all described with 6 directions. And except for gears and bearings that are described in lumped parameters, other subsystems are all modeled as continuums. Because the gear transmission error excitation is the main reason for gearbox vibration, only this excitation is applied on the gear system to simplify the problem. The aim of this paper is to study the vibratory

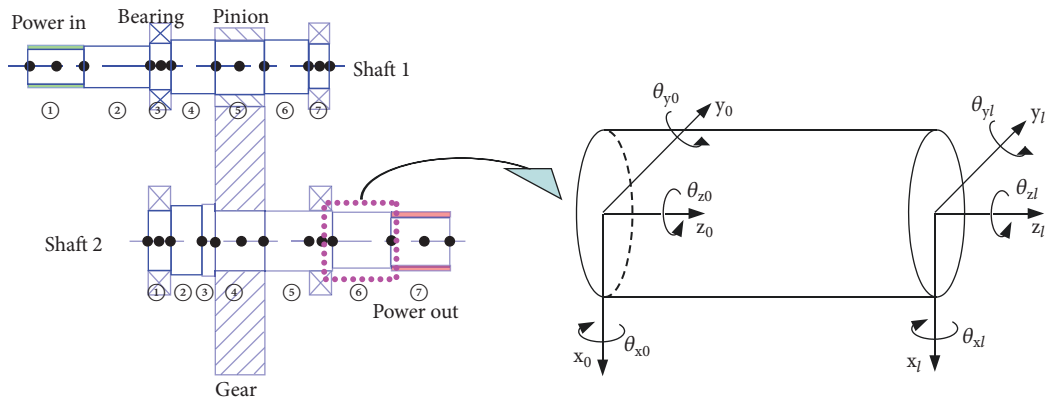

Figure 2: Model of the shaft structure.

Table 1: Basic gear parameters.

Tooth number	Normal module	Pressure angle	Helix angle	Face width
24 / 79	3 mm	20°	15.09°	45 mm

power transmission in the gear-housing-foundation coupled system and find main factors that influence the vibration of the foundation. So the back-reaction of flexible support on the gear mesh is ignored.

2.1. Gear Pair. The dynamic model of gear pairs has been extensively studied, and a time-varying mesh stiffness model [3] is adopted here. Basic gear parameters are listed in Table 1. The rotational speed of the pinion ranges from 50 to 15000 r/min, and the driven torque of the gear is 300 N·m.

The equation of motion of the gear pair is given by

$$\mathbf{M}\ddot{\mathbf{x}}(t) + \mathbf{C}\dot{\mathbf{x}}(t) + \mathbf{K}(t)(\mathbf{x}(t) - \mathbf{e}(t)) = \mathbf{f}^{\mathbf{GP}}(t), \quad (1)$$

where $\mathbf{M}$ is the mass matrix, $\mathbf{K}(t)$ is the stiffness matrix, $\mathbf{C}$ is the damping matrix, $\mathbf{e}(t)$ is the equivalent displacement vector of composite mesh error, $\mathbf{f}^{\mathrm{GP}}$ is the external force vector applied on the gear pair, that is, the dynamic reaction force applied by the shafts here, and $\mathbf{x}$, $\dot{\mathbf{x}}$, and $\ddot{\mathbf{x}}$ are the displacement vector, the velocity vector, and the acceleration vector, respectively.

Eq. (1) can be approximated as [6]

$$\mathbf{M}\ddot{\mathbf{x}}(t) + \mathbf{C}\dot{\mathbf{x}}(t) + \mathbf{K}_0\mathbf{x}(t) = \mathbf{f}^{\mathbf{GP}} + \mathbf{f}^{mesh}, \quad (2)$$

where $\mathbf{K}_0$ is the average part of the stiffness matrix, $\mathbf{f}^{mesh} = -\Delta\mathbf{K}(t)\cdot\mathbf{x}_s(t) + \mathbf{K}(t)\cdot e(t)$ is the transmission error excitation force vector, $\Delta\mathbf{K}(t)$ is the fluctuating component of the stiffness matrix, and $\mathbf{x}_s(t)$ is the static transmission error vector.

Eq. (2) can be transformed into the impedance equation of gear pair in the frequency domain [6]

$$\mathbf{Z}^{GP}\mathbf{V}^{GP} = \mathbf{F}^{GP} + \mathbf{F}^{mesh}, \quad (3)$$

where $\mathbf{Z}^{GP}(\omega) = \mathrm{j}\omega\mathbf{M} + \mathbf{C} + \mathbf{K}_0/(\mathrm{j}\omega)$ is the impedance matrix, $\mathrm{j} = \sqrt{-1}$, ω is the circular frequency, $\mathbf{V}^{GP}(\omega) = \mathrm{j}\omega\mathbf{X}(\omega)$ is the velocity vector in the frequency domain, and $\mathbf{F}^{\mathrm{GP}}$ and $\mathbf{F}^{\mathrm{mesh}}$ are the external force vector and the transmission error excitation force in the frequency domain.

Table 2: Shaft segments dimensions (mm).

	No. 1	No. 2	No. 3	No. 4	No. 5	No. 6	No. 7
OD_1	30	38	40	48	48	48	40
L_1	50	62	18	41	45	41	18
OD_2	55	63	65	58	55	52	45
L_2	21	29	12	45	62	55	55

2.2. Shaft. The shafts are divided into numerous segments, and shaft segments' dimensions are listed in Table 2. L is the length and OD is the diameter of shaft segments, and subscripts 1 and 2 mean the input shaft and the output shaft, respectively. Ren [6] built a lumped parameter model for each segment. In order to achieve better accuracy, a continuous Timoshenko beam model [34] with 2 external nodes and 6 directions at each node is used here, as shown in Figure 2. A torque of 91.14 N·m is applied on the power-in point. The rotational DOF of the power-out point is constrained.

The relationship between the state vectors is [34]

$$\begin{Bmatrix}\mathbf{x}_l\\ \mathbf{F}_l\end{Bmatrix} = \begin{bmatrix}\mathbf{T}_{11} & \mathbf{T}_{12}\\ \mathbf{T}_{12} & \mathbf{T}_{12}\end{bmatrix}\begin{Bmatrix}\mathbf{x}_0\\ \mathbf{F}_0\end{Bmatrix}, \quad (4)$$

where $\mathbf{x}$ is the displacement vector, $\mathbf{F}$ is the force vector, and $\mathbf{T}$ is the dynamic transfer matrix.

Eq. (4) can be transformed as

$$\begin{Bmatrix}\mathbf{F}_0\\ \mathbf{F}_l\end{Bmatrix} = \begin{bmatrix}\mathbf{K}_{11} & \mathbf{K}_{12}\\ \mathbf{K}_{21} & \mathbf{K}_{22}\end{bmatrix}\begin{Bmatrix}\mathbf{x}_0\\ \mathbf{x}_l\end{Bmatrix}, \quad (5)$$

where $\mathbf{K}$ is the dynamic stiffness matrix that can be yielded from

$$\mathbf{K}_{11} = -\mathbf{T}_{12}^{-1}\mathbf{T}_{11}$$

$$\mathbf{K}_{12} = -\mathbf{T}_{12}^{-1}$$

$$\mathbf{K}_{21} = \mathbf{T}_{21} - \mathbf{T}_{22}\mathbf{T}_{12}^{-1}\mathbf{T}_{11}$$
$$\mathbf{K}_{22} = \mathbf{T}_{22}\mathbf{T}_{12}^{-1}. \tag{6}$$

When structure damping is adopted, the impedance matrix can be obtained from

$$\mathbf{Z} = \frac{\mathbf{K}(1 + j\eta)}{j\omega}, \tag{7}$$

where η is the loss factor.

Then the impedance equation yields

$$\mathbf{Z}^{Sh}\mathbf{V}^{Sh} = \mathbf{F}^{Sh}. \tag{8}$$

2.3. Bearing. Angular contact ball bearings are used here. Each bearing is modeled as a spring and a damper acting in parallel. In order to study the vibration transmission of bearings, a comprehensive bearing stiffness matrix is adopted. Bearing stiffness matrix is shown in (9); $\mathbf{K}_m$ is defined in (10). Detailed description and numerical scheme for $\mathbf{K}_m$ can be found in [35].

$$\mathbf{K} = \begin{bmatrix} \mathbf{K}_m & -\mathbf{K}_m \\ -\mathbf{K}_m & \mathbf{K}_m \end{bmatrix}. \tag{9}$$

$$\mathbf{K}_m = \begin{bmatrix} \dfrac{\partial F_{im}}{\partial \delta_{jm}} & \dfrac{\partial F_{im}}{\partial \beta_{jm}} \\ \dfrac{\partial M_{im}}{\partial \delta_{jm}} & \dfrac{\partial M_{im}}{\partial \beta_{jm}} \end{bmatrix}_{\{q\}_m} \quad (i, j = x, y, z). \tag{10}$$

When damping is considered, the bearing impedance matrix can be expressed as

$$\mathbf{Z} = \frac{\mathbf{K}}{j\omega} + \mathbf{C}. \tag{11}$$

Then the impedance equation of bearing is formulated as

$$\mathbf{Z}^{\mathbf{Br}}\mathbf{V}^{\mathbf{Br}} = \mathbf{F}^{\mathbf{Br}}. \tag{12}$$

2.4. Gearbox Housing. The housing is made of steel and the length×width×height is 410 mm×215 mm×330 mm. A FE model of the gearbox housing is built, as shown in Figure 3. The material density is 7850 kg/m^3, Young's modulus is 2.07×10^{11} Pa, Poisson's ratio is 0.3, and the viscous damping ratio is 2%. The housing is meshed with 4 nodes' tetrahedron element and with over 75,000 nodes and more than 310,000 elements. The bearing holes are coupled at external nodes that are connected with bearings, and the bolt holes are coupled at external nodes that are connected with isolators. The block Lanczos method is adopted to extract the modal parameters, and 500 order modes are solved.

The mobility matrix of the housing is expressed in (13). Ten external nodes with six DOF per node are used, so the total DOF of the mobility matrix is 60. Each mobility element can be solved from (14).

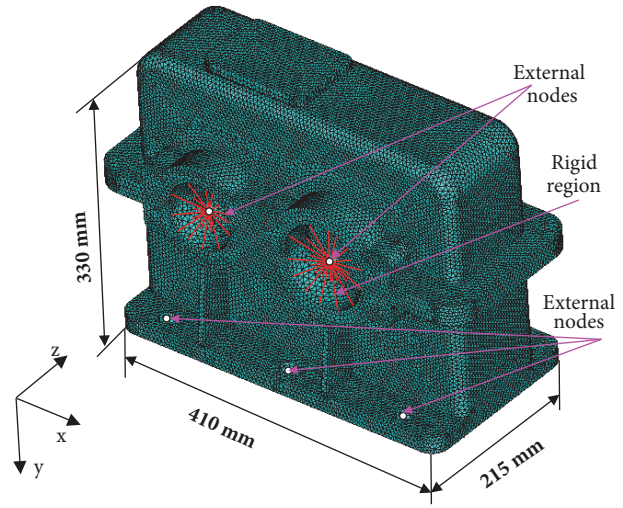

Figure 3: FE model of the housing.

$$\mathbf{Y} = \begin{bmatrix} Y_{11} & Y_{12} & \cdots & Y_{1n} \\ & Y_{22} & \cdots & Y_{2n} \\ & & \ddots & \vdots \\ Sym. & & & Y_{nn} \end{bmatrix}. \tag{13}$$

$$Y_{lp}(j\omega) = j\omega \sum_{r=1}^{n} \frac{u_l^r u_p^r}{K_r - \omega^2 M_r + j\omega C_r}, \tag{14}$$

where K_r is the modal stiffness, M_r is the modal mass, C_r is the modal damping, u is the modal shape, r means the mode order, and n is the number of modes.

The impedance matrix can be obtained through a matrix inversion of $\mathbf{Y}$

$$\mathbf{Z}^{\mathbf{GB}} = \mathbf{Y}^{-1}. \tag{15}$$

Then the impedance equation yields

$$\mathbf{Z}^{\mathbf{GB}}\mathbf{V}^{\mathbf{GB}} = \mathbf{F}^{\mathbf{GB}}. \tag{16}$$

2.5. Isolators. The isolator is made of rubber. It is modeled as a cylinder with a diameter of 40 mm and a height of 40 mm. The material density is 1000 kg/m^3, Young's modulus is 1×10^7 Pa, Poisson's ratio is 0.47, and the loss factor is 0.1.

A traditional isolator model ignores its mass, representing the isolator with pure spring stiffness and viscous damping in one direction. In order to study the wave effects, idealized "long-rod" models are introduced by previous researchers. Here, a more precise continuous Timoshenko beam model with six directions is adopted.

The impedance matrix of a continuous Timoshenko beam can be obtained from (7). Since the coordinates of the shaft and the isolator are different, a transformation has to be

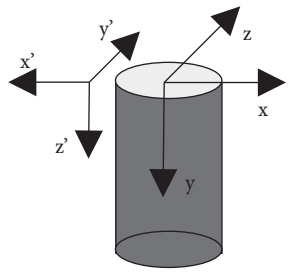

Figure 4: Model of the isolator structure.

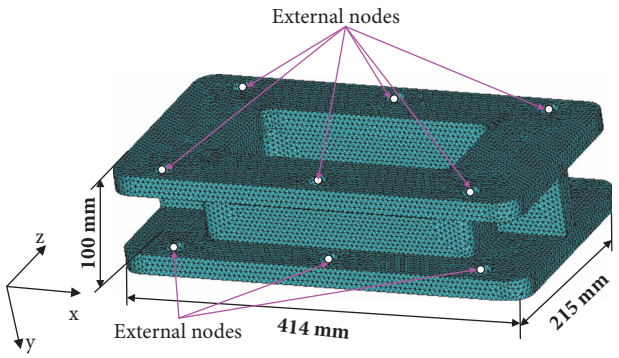

Figure 5: FE model of the raft.

carried out. The coordinates are shown in Figure 4; x'y'z' is the local coordinate, and xyz is the global coordinate.

$$\mathbf{Z} = \mathbf{\Lambda}^{\mathrm{T}} \mathbf{Z}' \mathbf{\Lambda}. \tag{17}$$

Z is the impedance matrix in the global coordinate, Z' is the impedance matrix in the local coordinate, Λ is the transform matrix and $\mathbf{\Lambda} = \mathrm{diag}(\boldsymbol{\gamma}, \boldsymbol{\gamma}, \boldsymbol{\gamma}, \boldsymbol{\gamma})$, and $\boldsymbol{\gamma}$ is the matrix that transforms from the global coordinate to the local coordinate, as expressed in the following equation.

$$\begin{Bmatrix} x' \\ y' \\ z' \end{Bmatrix} = [\boldsymbol{\gamma}] \begin{Bmatrix} x \\ y \\ z \end{Bmatrix} = \begin{bmatrix} -1 & 0 & 0 \\ 0 & 0 & 1 \\ 0 & 1 & 0 \end{bmatrix} \begin{Bmatrix} x \\ y \\ z \end{Bmatrix}. \tag{18}$$

2.6. Raft. The FE model of the raft is shown in Figure 5. The material is aluminum alloy, the density is 2700 kg/m3, Young's modulus is 7×10^{10} Pa, Poisson's ratio is 0.33, and the viscous damping ratio is 2%. The raft is meshed with 4 nodes' tetrahedron element with over 44,000 nodes and more than 210,000 elements. The bolt holes are coupled at external nodes that are connected with isolators. Over 500 order modes are solved in ANSYS software. The impedance matrix can be solved through (13)-(15).

The impedance equation of the raft is given by

$$\mathbf{Z}^{\mathbf{R}} \mathbf{V}^{\mathbf{R}} = \mathbf{F}^{\mathbf{R}}. \tag{19}$$

2.7. Foundation. The gearbox foundation in a ship usually has large size and complex structure. In this case the mobility of the foundation has to be measured directly from an experiment. Here a simple structure is used and the impedance can be yielded through its FE model. The FE model of the foundation is shown in Figure 6. The material is aluminum alloy, the density is 2700 kg/m^3, Young's modulus is 7×10^{10} Pa, Poisson's ratio is 0.33, and the viscous damping ratio is 2%. The foundation is meshed with 4 nodes' tetrahedron element with over 61,000 nodes and more than 265,000 elements. The bolt holes on the top area are coupled at external nodes that are connected with isolators. The bottom area is constrained for all DOFs. Over 500 order modes are solved in ANSYS software. The impedance matrix can be yielded from (13)-(15).

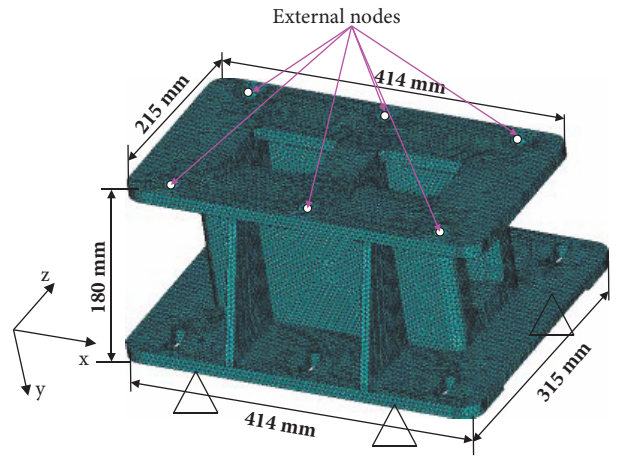

Figure 6: FE model of the foundation.

The impedance equation of the foundation yields

$$\mathbf{Z}^{\mathbf{F}} \mathbf{V}^{\mathbf{F}} = \mathbf{F}^{\mathbf{F}}. \tag{20}$$

2.8. Coupled Model. Impedance synthesis approach [6] is introduced to establish the impedance equation of the whole system. When dynamic models of all subsystems are built, coupled system impedance equation can directly be obtained by assembling impedance matrix elements according to the node number. In a general isolation model, the housing is treated as a rigid mass, and a unit force is applied on its centre of gravity. Here, the mesh transmission error excitation with 12 DOF obtained from the LTCA model in Section 2.1 is applied on the gear pair. Assume no external force acting at the interfaces between subsystems. The impedance equation of the coupled system can be obtained as follows:

$$\mathbf{ZV} = \mathbf{F}. \tag{21}$$

Impedance Z and force F in (21) are known, so velocity can be solved from the equation below:

$$\mathbf{V}(\omega) = \mathbf{Z}(\omega)^{-1} \mathbf{F}(\omega). \tag{22}$$

Displacement and acceleration can be yielded from (23) and (24), respectively.

$$\mathbf{X}(\omega) = \frac{\mathbf{V}(\omega)}{\mathrm{j}\omega}. \tag{23}$$

$$\mathbf{A}(\omega) = \mathrm{j}\omega \mathbf{V}(\omega). \tag{24}$$

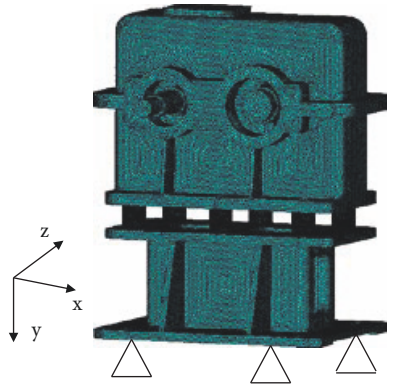

Figure 7: FE model of the coupled system.

In the time domain, the displacement, velocity, and acceleration can be obtained from the following equations, respectively.

$$\mathbf{x}(t) = \mathbf{x}_0 + \sum_{i_{GP}=1}^{n_{GP}} \sum_{k=1}^{K} \mathbf{X}\left(k \cdot \omega_{i_{GP}}\right) \cdot e^{\mathrm{j}k\omega_{i_{GP}}t}, \tag{25}$$

$$\mathbf{v}(t) = \sum_{i_{GP}=1}^{n_{GP}} \sum_{k=1}^{K} \mathbf{V}\left(k \cdot \omega_{i_{GP}}\right) \cdot e^{\mathrm{j}k\omega_{i_{GP}}t}, \tag{26}$$

$$\mathbf{a}(t) = \sum_{i_{GP}=1}^{n_{GP}} \sum_{k=1}^{K} \mathbf{A}\left(k \cdot \omega_{i_{GP}}\right) \cdot e^{\mathrm{j}k\omega_{i_{GP}}t}, \tag{27}$$

where x_0 is the static displacement, i_{GP} is the index of gear pairs, n_{GP} is the number of gear pairs, k is the index of harmonic component, K is the maximum harmonic order, $\mathrm{j} = \sqrt{-1}$, and $\omega_{i_{GP}}$ is the mesh frequency of the gear pair i_{GP}.

2.9. Comparison with the FE Model. Since the single-stage isolation configuration is currently most used, comparison and parametric study are both based on this model in this paper. A coupled FE model is built in ANSYS software, as shown in Figure 7. The gear pair is treated as a lumped parameter model with the mass and stiffness matrix given in (2). Bearings are modeled as springs with the stiffness matrix given in (9). The shafts, housing, isolators, and foundation are represented with 4-node tetrahedron elements with a maximum element size of 5 mm. The shaft and housing are made of steel and the foundation is made of aluminum alloy. The bottom area of the foundation is fixed to the ground. A 2% viscous damping ratio is used for the coupled system. The transmission error excitation force $\mathbf{F}^{\mathrm{mesh}}$ is applied on the gear nodes. The block Lanczos method is used to extract the modal parameters with 1000 orders and the modal superposition method is adopted to solve the harmonic analysis. Since the modal truncation will induce errors, it is almost impossible for the FE model to solve the dynamic response when the isolators are too soft. So Young's modulus of the isolators is changed to 10^9 Pa in this section.

The structure-borne noise of the housing and the foundation is solved by both the FE model and the impedance model.

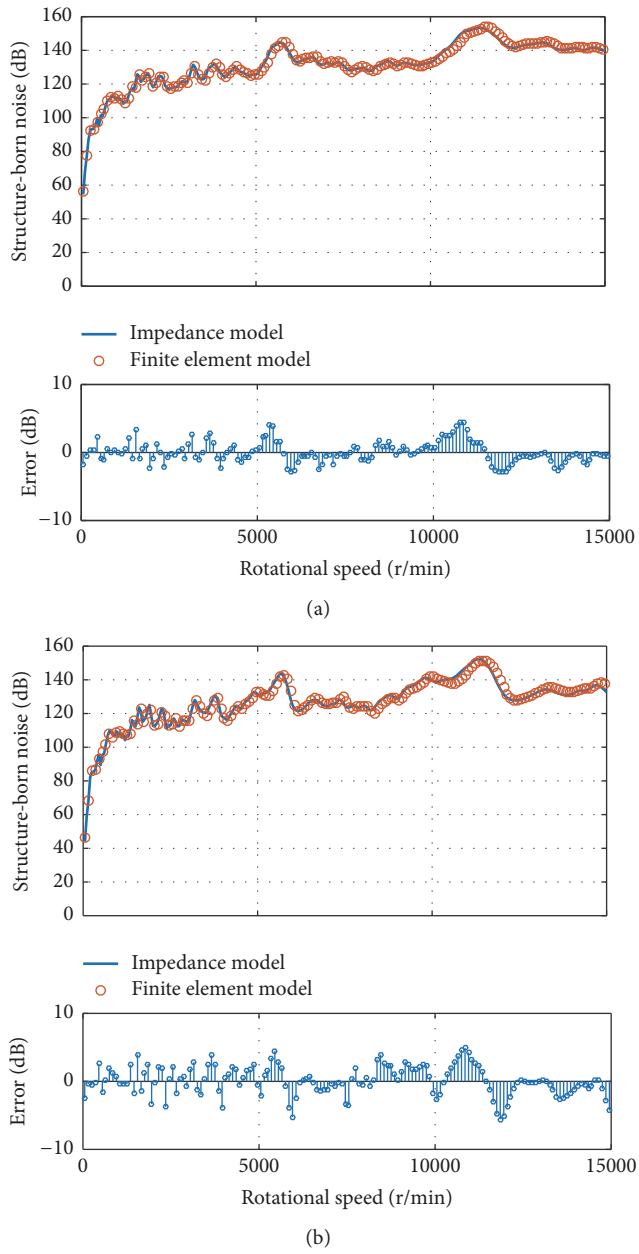

Figure 8: Comparison between the FE model and the impedance model: (a) vibration of the housing; (b) vibration of the foundation.

A good consistency between the two methods is shown in Figures 8(a) and 8(b). The error is caused by modal truncation in the FE model and the difference between system damping. Compared with the FE model, the impedance model is easy modeling and time saving.

3. Power Flow Analysis of Different Isolation Types

Power flow is the mean value of the transient power in one period. Because this scalar takes both force and velocity into consideration, it is more comprehensive in the describing of

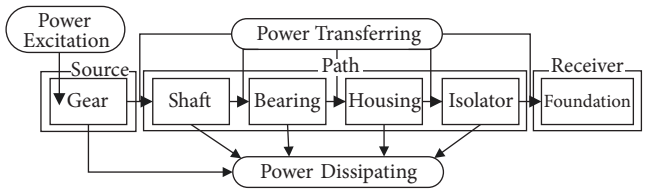

Figure 9: Scheme of the vibratory power flow in the single-stage isolation system.

vibration isolation performance than the force transmissibility or vibration level difference. Moreover, it can make an overall consideration of different DOF and especially can unitize the measurement between translational and rotational DOF. Furthermore, the transmitted power from the machine to the supporting structure is closely related to the structural noise emission from the supporting structure. Thus this index is widely used in vibration analysis and control.

In a whole gear-housing-foundation system, each subsystem will transfer and dissipate energy. Vibratory power flow of the single-stage isolation system shown in Figure 1(b) is taken as an example to illustrate the power flow scheme, as shown in Figure 9. The vibratory power is excited by the gear transmission error. The power then is transferred from the gear to the shaft, bearing, housing, isolator, and the foundation. During the propagation process, part of the energy is dissipated by system damping, and the rest is transmitted to the foundation which causes ship vibration and noise. The aim of vibration isolation is to reduce the vibratory power transmitted into the foundation.

Vibratory power flow of each frequency can be computed from (28) and the total vibration power can be yielded by adding power flows at all excitation frequencies and all directions.

$$\mathbf{P}_i = \frac{1}{2}\mathrm{Re}\left(\mathbf{v}_i^{\mathrm{H}} \cdot \mathbf{F}_i\right), \quad i = 1, 2, \ldots, n, \tag{28}$$

where $\mathbf{P}_i$ is the power flow through any interface of the ith subsystem, n is the number of subsystems, Re$(*)$ means the real part of $*$, H denotes the Hermitian transpose, and $\mathbf{F}_i$ and $\mathbf{v}_i$ are the force vector and the velocity vector, respectively.

Power dissipation in this paper refers to the power flow transmissibility of each subsystem,

$$D_P = 10\log\_10\left(\frac{P_{\mathrm{in}}}{P_{\mathrm{out}}}\right), \tag{29}$$

where P_{in} and P_{out} are the power transmitted in and out the subsystem, respectively. For example, for the power dissipation of the shaft, P_{in} means vibratory power transmitted from the gear to the shaft and P_{out} means vibratory power transmitted from the shaft to the bearing.

The vibratory power flows for the three different installation types, i.e., rigid installation, single-stage isolation, and double-stage isolation in Figures 1(a)–1(c), are computed under different rotational speeds ranging from 50 r/min to 15000 r/min (the corresponding gear mesh frequency ranged from 20 Hz to 6000 Hz). Results are shown in Figures 10, 11, and 12, respectively.

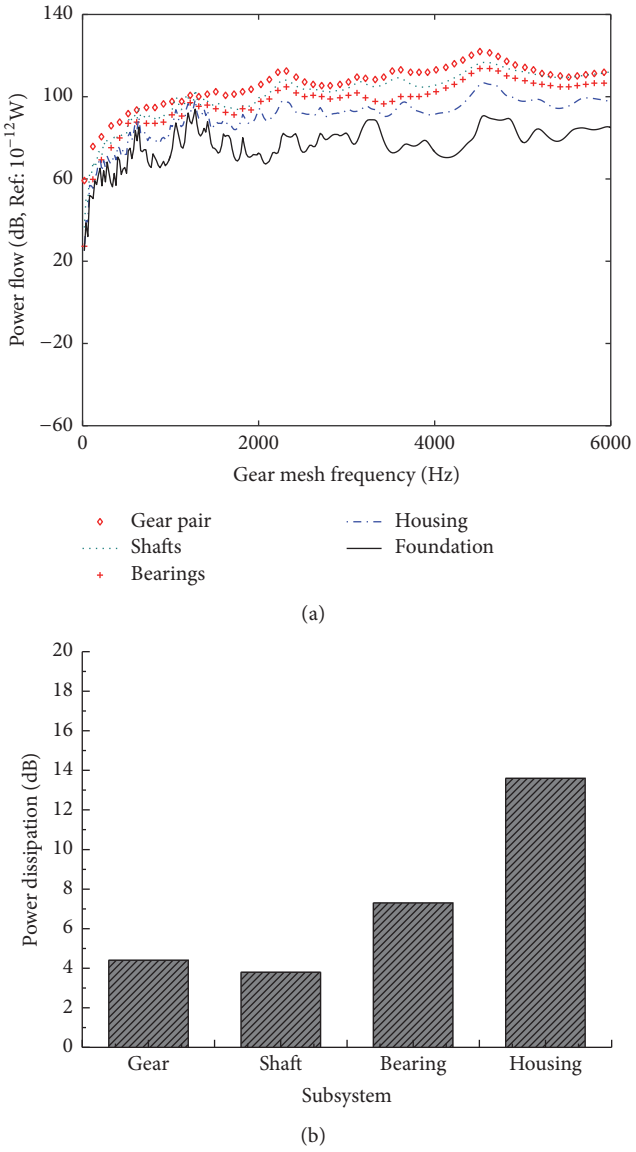

Figure 10: Vibratory power flow of the rigid installation system: (a) vibratory power flow; (b) average power dissipation.

Vibratory power flow of each subsystem in the rigid installation system is shown in Figure 10(a). As the rotational speed or gear mesh frequency increases, power transmitted to each subsystem increases on the whole. Each component can reduce the transmitted power, and the vibratory power gradually decreases from the gear to the foundation. However the energy dissipation is not obvious near some critical speed due to the influence of system resonance. The average power excited by the gear pair is 106.2 dB. And the power transmitted to the shaft, bearing, housing, isolator, and foundation is 101.8 dB, 98.0 dB, 90.7 dB, and 77.1 dB, respectively. The average power dissipation of each subsystem is shown in Figure 10(b). Power is mainly dissipated by the housing and the bearing for the rigid installation system.

Vibratory power flow of the single-stage isolation system is shown in Figure 11(a). The gear excitation power almost

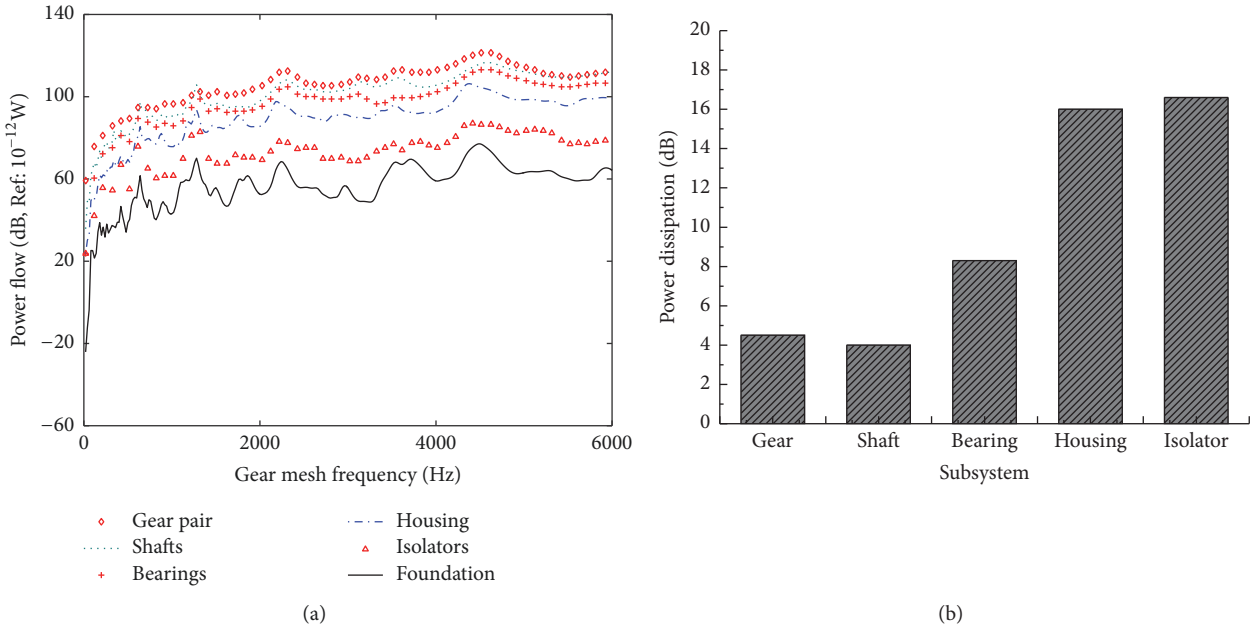

FIGURE 11: Vibratory power flow of the single-stage isolation system: (a) vibratory power flow; (b) average power dissipation.

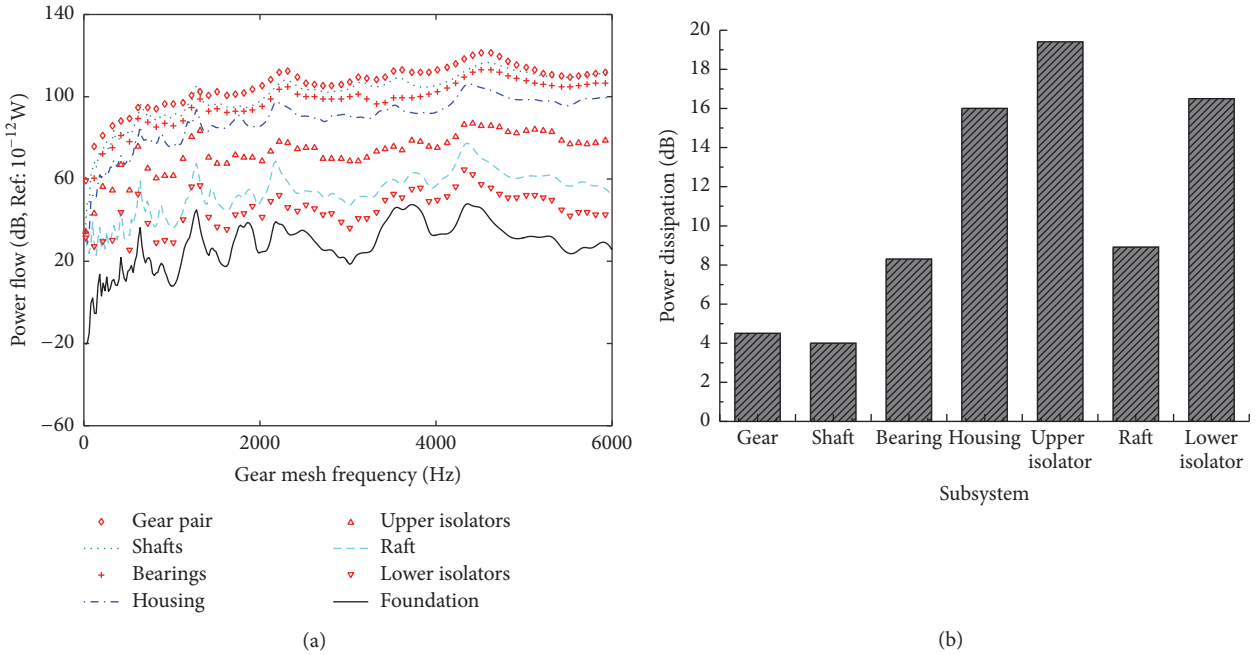

FIGURE 12: Vibratory power flow of the double-stage isolation system: (a) vibratory power flow; (b) average power dissipation.

unchanged but the power transmitted to the foundation decreased dramatically compared with the rigid installation case shown in Figure 10(a). Average power transmitted to the shaft, bearing, housing, isolator, and foundation is 101.6 dB, 97.6 dB, 89.3 dB, 73.4 dB, and 56.8 dB, respectively. The average power dissipation of each subsystem is shown in Figure 11(b). Compared with rigid installation case, power dissipated by the housing increased from 13.6 dB to 16.0 dB, and a new subsystem, i.e., isolator, can also dissipate power. Main components that dissipate vibratory power are the bearing, housing, and isolator for the single-stage isolation system.

Vibratory power flow of the double-stage isolation system is shown in Figure 12(a). The gear excitation power is almost the same as the rigid installation case and the single-stage isolation one. Average power transmitted to the shaft,

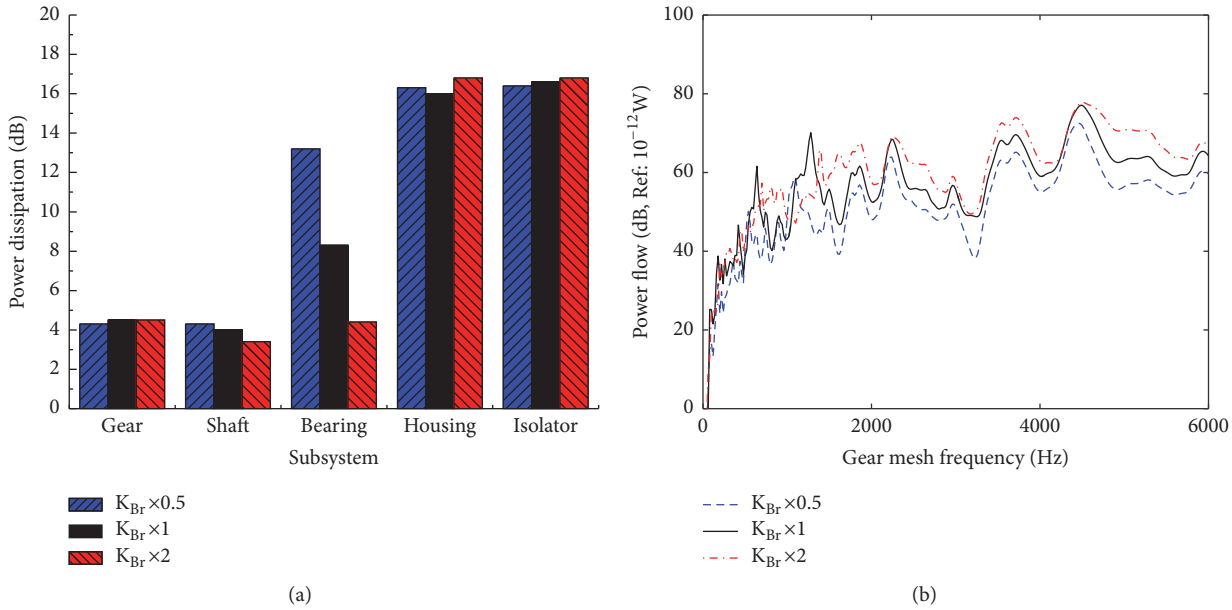

Figure 13: Influence of bearing stiffness on power flow: (a) average power dissipation; (b) power into the foundation.

bearing, housing, upper isolator, raft, lower isolator, and foundation is 101.6 dB, 97.7 dB, 89.4 dB, 73.4 dB, 53.9 dB, 45.1 dB, and 28.6 dB, respectively. The average power dissipated by each subsystem is shown in Figure 12(b). The bearing, housing, isolator, and raft play important roles in the power dissipation.

Comparison of power flow into the foundation between different installations types shows that power flow transmitted to the foundation in the single-stage isolation system is significantly lower than that in the rigid installation system, and the double-stage isolation system is more excellent than the single-stage isolation system. The mean power effectiveness is −20.3 dB and −48.5 dB for the single-stage isolation system and the double-stage isolation case, respectively.

4. Parametric Studies

Since the single-stage isolation system is currently the most widely used isolation type for a marine gearbox, the configuration shown in Figure 1(b) is taken as an example to study the parametric influence. Effects of the bearing stiffness, Young's modulus of the isolator, and the damping of each subsystem on the system vibratory power flow are analyzed.

4.1. Bearing Stiffness. In order to study the influence of bearing stiffness on the system power flow, the bearing stiffness is multiplied by 0.5 and 2, respectively. The power flow excited by the gear pair almost keeps unchanged when the bearing stiffness changes.

Influence of bearing stiffness on the subsystems' power flow dissipation is shown in Figure 13(a). On the one hand, increasing of bearing stiffness weakens the impedance mismatch between the shaft and the bearing and thus decreases the wave reflection and deteriorates the vibration isolation of the shaft; on the other hand, increase in bearing stiffness rapidly decreased the power dissipation of bearing. Influence of bearing stiffness on the power flow of the foundation is shown in Figure 13(b). Increasing bearing stiffness is harmful to vibration isolation on the whole. Power flow transmitted into the foundation increases as much as 18.1 dB at 1620 Hz for the stiffened case and decreases as much as 22.6 dB at 1280 Hz for the softened case. However, increase in bearing stiffness will change the system mode and thus may decrease vibration at some low frequencies. For example, vibration decreased 15.9 dB at 1280 Hz for the stiffened case and increased 10.4 dB at 1020 Hz for the softened case.

4.2. Young's Modulus of Isolator. Young's modulus of the isolator is multiplied by 0.5 and 2, respectively, in order to study the influence of isolators' stiffness on system vibration. Excitation power flow of the gear pair remains 105.9 dB.

Average power flow dissipation of subsystems is shown in Figure 14(a). On the one hand, increase in Young's modulus decreases the impedance mismatch between the housing and isolator and thus weakens the vibration isolation of the housing; on the other hand, increasing Young's modulus of isolator is harmful to its energy dissipation. Effect of Young's modulus of the isolator on the foundation's power flow is shown in Figure 14(b). On the whole, a large Young's modulus of the isolator will cause a large vibration. Power flow transmitted into the foundation increased as much as 13.9 dB at 1680 Hz when the isolator is stiffened and decreased as much as 13.3 dB at 1260 Hz when the isolator is softened. However, due to the change of system modes, increasing Young's modulus may reduce power flow transmitted into the foundation at some low frequencies. For example, increase

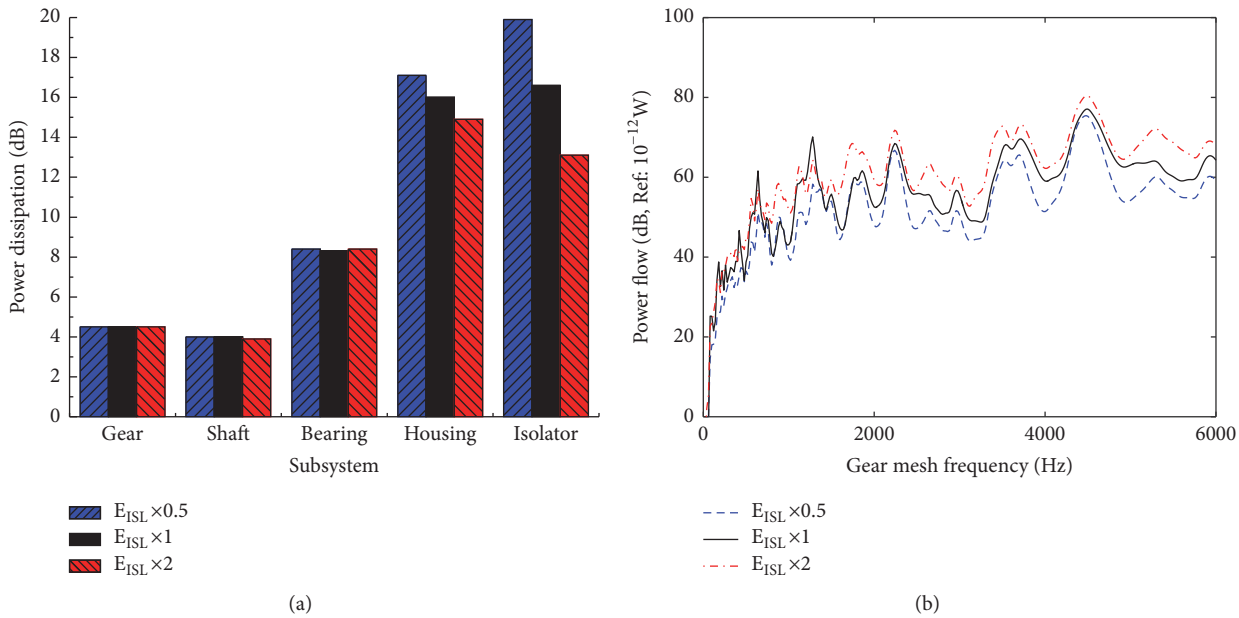

Figure 14: Influence of Young's modulus of isolator on power flow: (a) average power dissipation; (b) power into the foundation.

in isolator Young's modulus can decrease 6.4 dB system vibration at 1260 Hz, and decrease in Young's modulus can increase 3.1 dB at 860 Hz.

4.3. Subsystem Damping. In order to study the influence of system damping on the vibration, each subsystem damping is multiplied by 0.5 and 2, respectively. Power flow into the foundation is shown in Figure 15.

Influence of mesh damping on the power into the foundation is shown in Figure 15(a). Increase in mesh damping will decrease vibration near the gear-led resonance frequency and has little influence at other frequencies. Power transmitted into the foundation decreased 4.6 dB at 4560 Hz when the mesh damping is increased and increased 3.7 dB at 4560 Hz when the damping is decreased.

Damping of shaft and bearing have little influence on the foundation vibration, as shown in Figures 15(b) and 15(c).

The housing damping's influence on the foundation vibration is shown in Figure 15(d). Increase in housing damping will decrease vibration at middle and high frequencies, especially near system resonance. Power into the foundation decreased 6.7 dB at 3500 Hz when the housing damping is multiplied by 2.

Influence of isolator damping on the power flow into foundation is shown in Figure 15(e). Increase in the isolator damping can significantly decrease system vibration. Power flow transmitted into the foundation decreased 7.2 dB at 5040 Hz when the isolator damping is increased.

The foundation damping's influence on system vibration is shown in Figure 15(f). Increase in the foundation damping will decrease vibration near resonance frequencies but deteriorate vibration at other frequencies. For example, when the damping is increased, system vibration decreased 2.2 dB at 4520 Hz and increased 2.6 dB at 4160 Hz.

5. Conclusions

In order to study the vibration transmission in the marine gearbox, dynamic models of gear, shaft, bearing, housing, isolator, raft, and foundation are built, respectively, and impedance synthesis approach is adopted to constitute a whole gear-housing-foundation coupled system. The static transmission error excitation is applied on the model. Power flow index is used to measure the vibration transmission performance. Specific conclusions are listed below.

(1) The proposed impedance synthesis model is able to couple gear system with the vibration isolation system. This model with multimount, multidirection, and flexible component can more comprehensively illustrate the vibration propagation in a marine gearbox.

(2) Power flows of three isolation configurations are studied. The single-stage isolation system is superior to the rigid installation system, and the double-stage isolation system is better than the single-stage isolation system. The average power flow effectiveness for the single-stage isolation system and the double-stage isolation system is −20.3 dB and −48.5 dB, respectively. The housing and isolator are the main component to dissipate power, while the gear and shaft have limited contribution.

(3) Increasing the bearing stiffness and Young's modulus of the isolator are harmful to vibration isolation, while increasing the housing damping and the isolator damping are beneficial to vibration reduction. Increasing the damping of the gear pair, shaft, and bearing can hardly affect the power flow transmitted to the foundation.

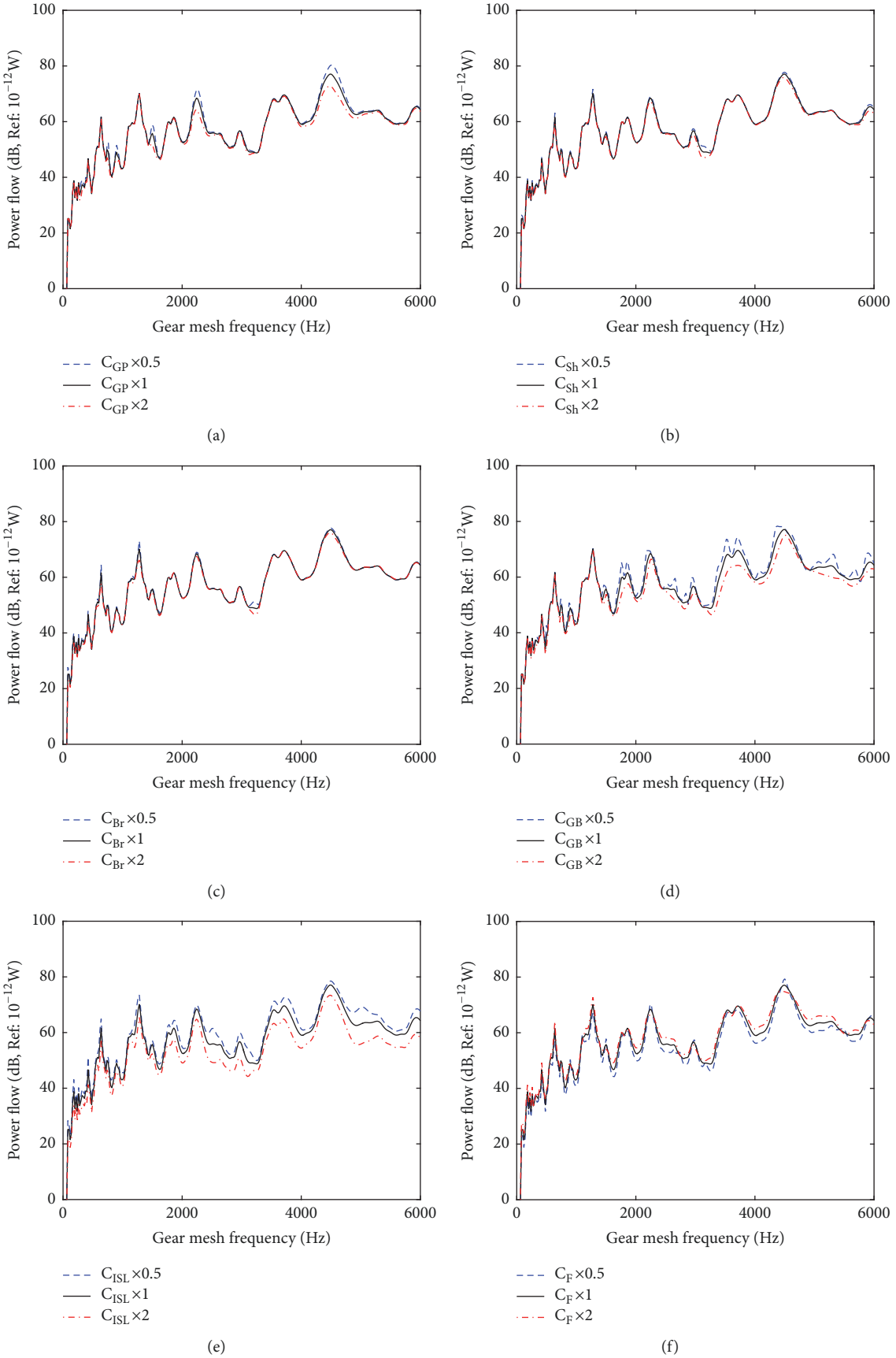

FIGURE 15: Influence of subsystem damping on power flow into the foundation: (a) gear pair; (b) shaft; (c) bearing; (d) housing; (e) isolator; (f) foundation.

Nomenclature

e:	Equivalent displacement of composite mesh error
f^{mesh}:	Transmission error excitation
F:	Force vector
j:	$\sqrt{-1}$
K_0:	Average mesh stiffness
$\Delta\mathbf{K}$:	Fluctuating component of mesh stiffness
D_P:	Power dissipation
M, C, K:	Mass, damping, and stiffness matrix
M_r, C_r, K_r:	Modal mass, modal damping, and modal stiffness
P:	Power flow
T:	Dynamic transfer matrix
U:	Modal shape
x, v, a:	Displacement, velocity, and acceleration in the time domain
x_s:	Static transmission error
X, V, A:	Displacement, velocity, and acceleration in the frequency domain
Y:	Mobility matrix
Z:	Impedance matrix
η:	Loss factor
Λ:	Transformation matrix
ω:	Circular frequency.

Superscript

GP:	Gear pair
Sh:	Shaft
Br:	Bearing
GB:	Gearbox or housing
ISL:	Isolator
UISL:	Upper layer isolator
LISL:	Lower layer isolator
R:	Raft
F:	Foundation
H:	Hermitian transpose.

Subscript

b: Bottom
t: Top
r: Receiver
s: Source.

Conflicts of Interest

The authors declare that there are no conflicts of interest regarding the publication of this paper.

Acknowledgments

This study is supported by the Key Project of National Science Foundation of China (Grant no. 51535009) and 111 Project (Grant no. B13044), China.

References

[1] T. Kiekbusch, D. Sappok, B. Sauer, and I. Howard, "Calculation of the combined torsional mesh stiffness of spur gears with two- and three-dimensional parametrical FE models," *Strojniški Vestnik-Journal of Mechanical Engineering*, vol. 57, no. 11, pp. 810–818, 2011.

[2] R. G. Parker, V. Agashe, and S. M. Vijayakar, "Dynamic response of a planetary gear system using a finite element/contact mechanics model," *Journal of Mechanical Design*, vol. 122, no. 3, pp. 304–310, 2000.

[3] L. Chang, G. Liu, and L. Wu, "A robust model for determining the mesh stiffness of cylindrical gears," *Mechanism and Machine Theory*, vol. 87, pp. 93–114, 2015.

[4] Q. Wang and Y. Zhang, "A model for analyzing stiffness and stress in a helical gear pair with tooth profile errors," *Journal of Vibration and Control*, vol. 23, no. 2, pp. 272–289, 2017.

[5] S. Xue and I. Howard, "Dynamic modelling of flexibly supported gears using iterative convergence of tooth mesh stiffness," *Mechanical Systems and Signal Processing*, vol. 80, pp. 460–481, 2016.

[6] Y. Ren, S. Chang, G. Liu, L. Wu, and T. C. Lim, "Impedance synthesis based vibration analysis of geared transmission system," *Shock and Vibration*, vol. 2017, Article ID 4846532, 14 pages, 2017.

[7] J. Yang and T. C. Lim, "Nonlinear dynamic simulation of hypoid gearbox with elastic housing," in *Proceedings of the ASME 2011 International Design Engineering Technical Conferences and Computers and Information in Engineering Conference, IDETC/CIE 2011*, pp. 437–447, usa, August 2011.

[8] H. Liu, C. Xiang, and S. Fu, "Research on dynamic coupled characteristics of a tracked vehicle gearbox," *International Journal of Computational Intelligence Systems*, vol. 4, no. 6, pp. 1204–1215, 2011.

[9] X. Xu, Y. Tao, C. Liao, S. Dong, and R. Chen, "Dynamic Simulation of Wind Turbine Planetary Gear Systems with Gearbox Body Flexibility," *Strojniški vestnik - Journal of Mechanical Engineering*, vol. 62, no. 11, pp. 678–684, 2016.

[10] Y. Guo, T. Eritenel, T. M. Ericson, and R. G. Parker, "Vibro-acoustic propagation of gear dynamics in a gear-bearing-housing system," *Journal of Sound and Vibration*, vol. 333, pp. 5762–5785, 2014.

[11] T. C. Lim and R. Singh, "Vibration transmission through rolling element bearings, part II: System studies," *Journal of Sound and Vibration*, vol. 139, no. 2, pp. 201–225, 1990.

[12] H. Xiao, X. Zhou, J. Liu, and Y. Shao, "Vibration transmission and energy dissipation through the gear-shaft-bearing-housing system subjected to impulse force on gear," *Measurement*, vol. 102, pp. 64–79, 2017.

[13] T. E. Rook and R. Singh, "Mobility analysis of structure-borne noise power flow through bearings in gearbox-like structures," *Noise Control Engineering Journal*, vol. 44, no. 2, pp. 69–78, 1996.

[14] R. C. N. Leung and R. J. Pinnington, "Vibrational power transmission of an idealized gearbox," *Journal of Sound and Vibration*, vol. 128, no. 2, pp. 259–273, 1989.

[15] J. S. Tao, G. R. Liu, and K. Y. Lam, "Design optimization of marine engine-mount system," *Journal of Sound and Vibration*, vol. 235, no. 3, pp. 477–494, 2000.

[16] R. Alkhatib, G. N. Jazar, and M. F. Golnaraghi, "Optimal design of passive linear suspension using genetic algorithm," *Journal of Sound and Vibration*, vol. 275, no. 3-5, pp. 665–691, 2004.

[17] S. Xie, S. W. Or, H. Lai Wa Chan, P. Kong Choy, and P. Chou Kee Liu, "Analysis of vibration power flow from a vibrating machinery to a floating elastic panel," *Mechanical Systems and Signal Processing*, vol. 21, no. 1, pp. 389–404, 2007.

[18] W. J. Choi, Y. P. Xiong, and R. A. Shenoi, "Power flow analysis for a floating sandwich raft isolation system using a higher-order theory," *Journal of Sound and Vibration*, vol. 319, no. 1-2, pp. 228–246, 2009.

[19] J. Pan, J. Pan, and C. H. Hansen, "Total power flow from a vibrating rigid body to a thin panel through multiple elastic mounts," *The Journal of the Acoustical Society of America*, vol. 92, no. 2, pp. 895–907, 1992.

[20] J. I. Soliman and M. G. Hallam, "Vibration isolation between non-rigid machines and non-rigid foundations," *Journal of Sound and Vibration*, vol. 8, no. 2, pp. 329–351, 1968.

[21] N. M. M. Maia, J. M. M. Silva, and A. M. R. Ribeiro, "Transmissibility concept in multi-degree-of-freedom systems," *Mechanical Systems and Signal Processing*, vol. 15, no. 1, pp. 129–137, 2001.

[22] D. A. Swanson, L. R. Miller, and M. A. Norris, "Multidimensional mount effectiveness for vibration isolation," *Journal of Aircraft*, vol. 31, no. 1, pp. 188–196, 1994.

[23] P. Gardonio and S. J. Elliott, "Passive and active isolation of structural vibration transmission between two plates connected by a set of mounts," *Journal of Sound and Vibration*, vol. 237, no. 3, pp. 483–511, 2000.

[24] Y. Du, R. A. Burdisso, E. Nikolaidis, and D. Tiwari, "Effects of isolators internal resonances on force transmissibility and radiated noise," *Journal of Sound and Vibration*, vol. 268, no. 4, pp. 751–778, 2003.

[25] M. A. Sanderson, "Vibration isolation: Moments and rotations included," *Journal of Sound and Vibration*, vol. 198, no. 2, pp. 171–191, 1996.

[26] B. A. T. Petersson and B. M. Gibbs, "Use of the source descriptor concept in studies of multi-point and multi-directional vibrational sources," *Journal of Sound and Vibration*, vol. 168, no. 1, pp. 157–176, 1993.

[27] W. L. Li and P. Lavrich, "Prediction of power flows through machine vibration isolators," *Journal of Sound and Vibration*, vol. 224, no. 4, pp. 757–774, 1999.

[28] X.-T. Weng, R. Huo, S.-Y. Li, and C.-P. Liu, "Research on evaluation of vibration isolation efficiency based on power flow analysis," *Applied Mechanics and Materials*, vol. 590, pp. 149–154, 2014.

[29] H. L. Sun, H. B. Chen, K. Zhang, and P. Q. Zhang, "Research on performance indices of vibration isolation system," *Applied Acoustics*, vol. 69, no. 9, pp. 789–795, 2008.

[30] R. Singh and S. Kim, "Examination of multi-dimensional vibration isolation measures and their correlation to sound radiation over a broad frequency range," *Journal of Sound and Vibration*, vol. 262, no. 3, pp. 419–455, 2003.

[31] B. Niu and N. Olhoff, "Minimization of vibration power transmission from rotating machinery to a flexible supporting plate," *International Journal of Structural Stability and Dynamics*, vol. 14, no. 03, p. 1350068, 2014.

[32] J. Niu, K. Song, and C. W. Lim, "On active vibration isolation of floating raft system," *Journal of Sound and Vibration*, vol. 285, no. 1-2, pp. 391–406, 2005.

[33] Y. P. Xiong, X. P. Wang, J. T. Xing, and W. G. Price, "Hybrid active and passive control of vibratory power flow in flexible isolation system," *Shock and Vibration*, vol. 7, no. 3, pp. 139–148, 2000.

[34] B. Tang, "Dynamic analysis of crankshafts using dynamic stiffness matrix," *Chuan Bo Li Xue/Journal of Ship Mechanics*, vol. 13, no. 3, pp. 465–476, 2009.

[35] T. C. Lim and R. Singh, "Vibration transmission through rolling element bearings, part I: bearing stiffness formulation," *Journal of Sound and Vibration*, vol. 139, no. 2, pp. 179–199, 1990.